Structural Engineering and Mechanics, *Vol. 55, No. 2 (2015) 263-280*
DOI: http://dx.doi.org/10.12989/sem.2015.55.2.263

A finite element-experimental study of the impact of spheres on aluminium thin plates

Giancarlo B. Micheli[*1,2], Larissa Driemeier[2a] and Marcílio Alves[1b]

[1]*Group of Solid Mechanics and Structural Impact–GMSIE, Department of Mechatronics and Mechanical Systems Engineering, University of São Paulo, Av. Prof. Mello Moraes, 2231, 05508-900 São Paulo, SP, Brazil*
[2]*National Institute of Metrology, Quality and Technology–Inmetro, Av. N. Sa. das Graças, 50, 25250-020, Duque de Caxias, RJ, Brazil*

(Received July 20, 2013, Revised October 8, 2014, Accepted May 15, 2015)

Abstract. This paper describes a study of the collision of hard steel spheres against aluminium thin circular plates at speeds up to 140 m/s. The tests were monitored by a high speed camera and a chronoscope, which allowed the determination of the ballistic limit and the plate deformation pattern. Quasi-static material parameters were obtained from tests on a universal testing machine and dynamic mechanical characterization of two aluminium alloys were conducted in a split Hopkinson pressure bar. Using a damage model, the perforation of the plates was simulated by finite element analysis. Axisymmetric, shell and solid elements were employed with various parameters of the numerical analysis being thoroughly discussed, in special, the dynamic model parameters. A good agreement between experiments and the numerical analysis was obtained.

Keywords: impact tests; ballistic limit; dynamic material properties; numerical analysis

1. Introduction

Several studies on plate impact have been published along the years. The scientific and technological knowledge gained with these studies is quite broad but the complexity of the subject warrants further investigation. Issues like the influence of the projectile and plate geometry, boundary conditions and material characteristics on the ballistic limit are still the subject of various investigations.

The specialized literature covers many aspects of high velocity plate perforation. In a numerical and experimental study on plate perforation, Gupta *et al.* (2006) analysed the influence of the projectile shape on the ballistic limit of a 1 mm thick aluminium plate. Blunt nose projectiles penetrated more easily through the plates when compared to hemispherical noses. The residual velocity, i.e. the velocity of the projectile after perforation, was less sensitive to the projectile

∗Corresponding author, D.Sc., E-mail: gbmicheli@inmetro.gov.br
[a]Ph.D., E-mail: driemeie@usp.br
[b]Ph.D., E-mail: maralves@usp.br

http://www.techno-press.org/?journal=sem&subpage=8 ISSN: 1225-4568 (Print), 1598-6217 (Online)

shape and at impact velocities higher than 100 m/s the velocity reduction for both types of projectile were very similar. The numerical ballistic limit was determined within an error of around 10 %.

The impact of blunt-nosed cylindrical projectiles against steel plates was reported by Borvik *et al.* (1999). The residual projectile velocities plotted against the impact velocity had good agreement with a model proposed by Recht and Ipson (1963). Perforation occurred by detachment of a circular plug, which presented higher velocity than residual velocity of the projectile. The results also indicated that the amount of initial kinetic energy converted into target and projectile work decreases with increasing impact velocity. Borvik *et al.* (2002a) identified that the projectile shape significantly affects the plate failure mode and hence the residual velocity. The ballistic limits were the same for hemispherical and conical projectiles, which penetrated the target mainly by pushing aside the material in front of its tip, but the limit velocities were significantly different from the blunt ones.

Failure by plugging was also studied by Borvik *et al.* (1999, 2001a) with a viscoplastic damage finite element model. Numerical studies by Borvik *et al.* (2001b) explored the role of temperature, strain rate and finite element size on the plugging phenomenon. Sciuva *et al.* (2003) studied the impact behaviour of nickel IN718 5.5 mm and 11.95 mm thick, 170.0 mm square plates, subjected to low (6.0-7.0 m/s) and high (250.0-550.0 m/s) impact velocity of steel spherical projectiles. These tests were also simulated using shell and solid finite elements, with a better correlation between strain gauge signals and the solid finite element data. The analysis also disclosed small time intervals where the contact force was zero, leading to the conclusion that the projectile penetration occurs through various intermittent impacts.

Other studies (Borvik *et al.* 2002a, b) indicated that aluminium plates have a better mass-specific energy absorption performance than corresponding steel plates, and even better when compared to concrete plates. Borvik *et al.* (2005) studied the behaviour of extruded AA6005-T6 aluminium panels to the impact of ogival shape projectiles. The panels were made by two 6.0 mm thick cover plates set 130.0 mm apart by a W shaped profile made of 3.0 mm thick plates. The ballistic limit was measured and the perforation was by petal formation rather than by shear plugging. The simulation was carried out with solid finite elements, with an error of only 3 % for the ballistic velocity.

The influence of plate fixity conditions on ballistic performance were studied both experimentally and by finite element simulations by Tiwari *et al.* (2014). 1 mm thick aluminium plates were subjected to the impact of a blunt and an ogive nosed projectile. Decreasing the fixity region from 100 % until 25 % at the plate circumference the ballistic limit and global deformation of the targets increased. This effect was more prominent in the case of ogive projectile.

The phenomenon of plate perforation is further complicated by the local temperature increase in regions subjected to large sudden deformation. This leads to material softening, as explored in a numerical study by Yadav *et al.* (2001) with 6061-T6 aluminium panels and tungsten projectiles at velocities of the order of kilometres per second. It was indicated the necessity of considering the temperature influence on the material response in order to better represent the phenomenon, as similarly concluded by Kurtaran *et al.* (2003) when studying military vehicles protection. In contrast, Borvik *et al.* (1999), Gupta *et al.* (2006) indicated that the adiabatic temperature rise was not significant on tests in the range of hundreds meters per second. Holmen *et al.* (2013) concluded that material thermal softening used on numerical simulations of aluminium plate perforations by 7.62 mm APM2 bullets was the reason of differences from experimental tests.

The aim of this work is to investigate the perforation of thin plates by performing experimental

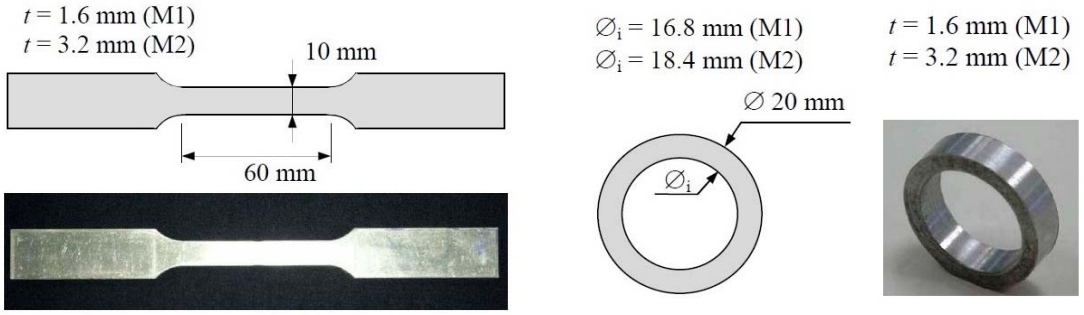

(a) Tensile test specimens (b) Compressive test specimens

Fig. 1 Specimens used on the tensile and compressive tests

tests and using finite element modelling with a damage model. A failure criterion based on equivalent plastic strain is also used. The parameters of the Continuum Damage Mechanics based criterion and the dynamic mechanical properties were measured for two aluminium alloy plates AL2524T3 and AL2024T3 of different thickness. Further, it was also investigated in detail how the various numerical parameters used by the finite element model influence the deformation and the failure predictions, in special, the dynamic model parameters. Numerical and experimental data were compared and the obtained ballistic limits showed good agreement.

2. Material characterization

Two aeronautic aluminium alloys, Al2524T3 and Al2024T3, were used to manufacture plates of thickness H=1.6 mm (plate M1) and H=3.2 mm (plate M2), respectively. The plates were used as targets to be impacted by a stainless steel sphere. Samples of these materials were used to machine tensile and compression specimens to obtain the quasi-static and dynamic mechanical properties. The results allowed the identification of various constitutive parameters.

2.1 Quasi-static material characterization

2.1.1 Tensile tests

The quasi-static mechanical behaviour of the M1 and M2 alloys was investigated using a tensile test machine and a standard tensile specimen presented in Fig. 1(a).

The load history was measured by a 50 kN load cell and the displacement by a 25 mm extensometer clipped to the specimen straight side. The specimens were cut in both the plate rolling direction and perpendicular to it. The tests were performed at 5.0 mm/min, giving a nominal strain rate of 0.0033 s^{-1}, with necking being rarely observed. The material responses in both rolling and perpendicular directions were similar. Thus, Young modulus, E, yield stress, σ_0, and strain rate, $\dot{\varepsilon}_p^0$, were obtained and are listed in Table 1.

The material plastic strength was assumed to be represented by

$$\sigma_y = \sigma_0 + Q_1\left[1 - \exp\left(-C_1\varepsilon_p\right)\right] \tag{1}$$

Table 1 Static, dynamic and damage parameters for alloys Al2524T3 and Al2024T3

Material	E (GPa)	σ_0 (MPa)	$\dot{\varepsilon}_p^0$ (10^{-3} s^{-1})	Q_1 (MPa)	C_1	Q_{1C} (MPa)	C_{1C}	S (MPa)	ε_p^D	D_C	V_k (MPa·s)	V_m
M1	73.39	351.7	3.22	156.5	24.6	188.7	9.41	3.3	0.05	0.19	15.02	0.23
M2	75.61	347.5	2.38	189.8	21.8	192.1	15.74	2.8	0.07	0.14	$1.26 \cdot 10^{-5}$	1.81

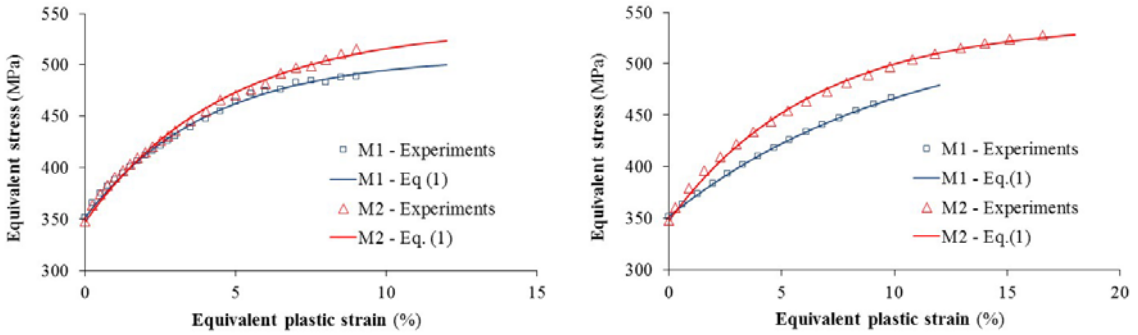

(a) Tensile tests (b) Compressive tests

Fig. 2 Average experimental and fitted data for the equivalent stress-equivalent plastic strain for materials M1 and M2

ε_p is the plastic strain, with Q_1 and C_1 being material parameters listed in Table 1 and calculated from the experimental data by using the simplex optimization method. Fig. 2(a) presents the experimental data and the fitted material model.

The Lemaitre damage model (Lemaitre 1992) was used to describe the onset of failure of the plates. It postulates that damage, D, evolves according to

$$\dot{D} = \begin{cases} 0, & \text{if } \varepsilon_p \le \varepsilon_p^D \\ \dfrac{Y}{S(1-D)}\dot{\varepsilon}_p, & \text{if } \varepsilon_p > \varepsilon_p^D \end{cases}, \tag{2}$$

with Y being the deformation energy release rate density, S is a material parameter and ε_p^D is the plastic deformation associated with the beginning of damage. The identification of the damage evolution for the two alloys was made by measuring the elastic modulus from cycles of load-unload at different plastic deformations of the two materials and using

$$\widetilde{E} = E(1-D), \tag{3}$$

where $\widetilde{E}$ is the actual Young modulus. The results are listed in Table 1, with D_c being the critical damage parameter associated with the tensile specimen close to the rupture state.

2.1.2 Compression tests

The third direction of the plates, perpendicular to its plane, was tested with compressive quasi-static loading to generate a quasi-static curve to be used as a reference for the dynamic tests.

Specimens of ring shape, presented in Fig. 1(b), all with external diameter of 20.0 mm and internal diameters of 18.4 mm and 16.8 mm, and thickness of 1.6 mm and 3.2 mm, for plates M1

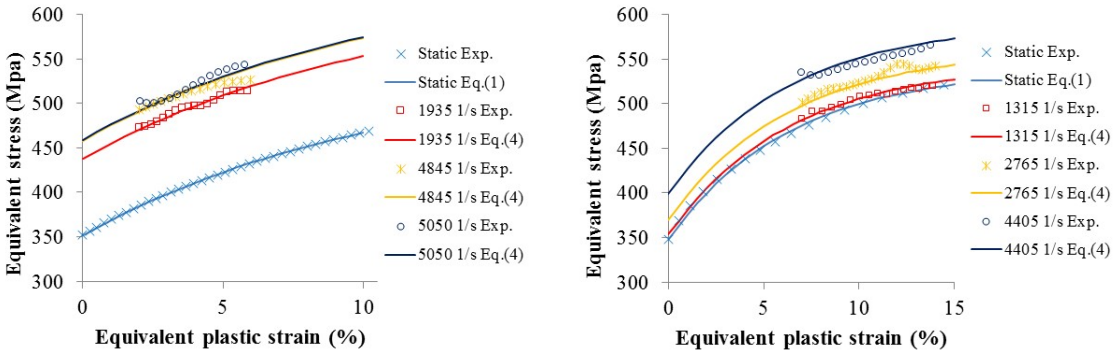

(a) M1 (b) M2

Fig. 3 Comparison between predicted and experimental curves for both materials

and M2, respectively, were compressed in the same machine used in the tensile tests. A load cell of 100 kN was used for the force measurement and a LVDT was used to obtain the displacement history. Average strain rates of $2.3 \cdot 10^{-4}$ s^{-1} and $2.6 \cdot 10^{-3}$ s^{-1} were measured for materials M1 and M2, respectively.

The strain hardening model described by Eq. (1) was adjusted with the optimization method, giving the parameters Q_{1C} and C_{1C} in Table 1. These parameters yield the curves in Fig. 2(b).

2.2 Dynamic material characterization

The dynamic material behaviour of alloys M1 and M2 was investigated with compressive tests in a conventional Split Hopkinson Pressure Bar, SHPB. The same ring geometry used in the compressive quasi-static tests were adopted. It has a ratio of 2.0 between the ring thickness and its external to internal radius difference. This is shown by Alves and Karagiozova (2007), Alves *et al.* (2012) to minimize friction effects between the bar ends and the specimen.

Conventional SHPB analysis (Song and Chen 2005) was adopted for this ring geometry, multiplying the calculated stress by a friction correction factor of 0.85 as discussed in Alves *et al.* (2012).

The measured curves are presented in Fig. 3. Three tests for each material were selected to determine the strain rate hardening parameters of the Cowper-Symonds model (Alves 2000), where the dynamic flow stress, σ_d, is

$$\sigma_d = \sigma_y \left[1 + \left(\frac{\dot{\varepsilon}_p}{C} \right)^{1/p} \right] = \sigma_y + V_k \dot{\varepsilon}_p^{V_m}, \tag{4}$$

whose parameters $V_k = \sigma_y (1/C)^{1/p}$ and $V_m = 1/p$ are listed in Table 1 for the two alloys. Fig. 3 also presents the predicted material curves based on the Cowper-Symonds parameters.

3. Impact tests

Thin plates made of materials M1 and M2 were tested using a gas gun operated by pressurized

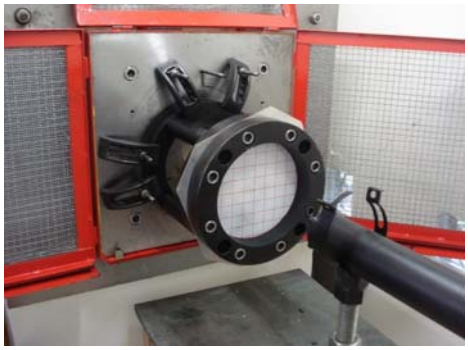

(a) Impact cage

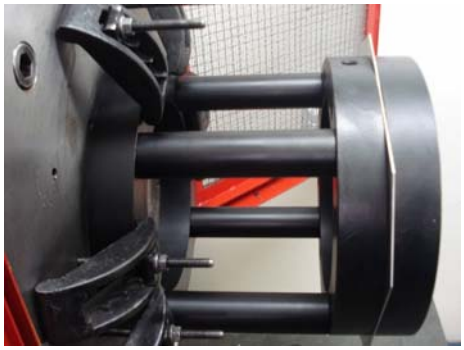

(b) Plate fixture set

Fig. 4 Impact cage opened and detail of target fixture

air. A fast response valve releases the air from the pressure vessel, accelerating a sabot and a projectile through a tube, whose end was near to the target. There is a safety cage located at the impacted end, as shown in Fig. 4(a). The hard steel spheres were 20.0 mm in diameter and reached velocities as high as 140.0 m/s, measured by a photodiode based apparatus. A nylon sabot was designed to guide the sphere through the tube and was stopped by an inertial mass at the tube end with a central hole slightly larger than the sphere.

The plates were sandwiched by two steel thick rings, which were tightened by eight bolts screwed by a pneumatic tool operating at 600 kPa. The rings, internal and external diameters of 250.0 mm and 350.0 mm, were fastened to a large inertial steel-concrete block. Thus, the panels became circular of diameter 250.0 mm and clamped as shown in Fig. 4(b).

By controlling the vessel air pressure, it was possible to change the impact velocity of the sphere. At low velocities, no fracture was detected and the maximum deformation was monitored. At higher velocities, the limit between the partial and total perforations was determined using a high speed camera, operating at a rate of 30,000 frames per second.

3.1 Deformation measurements

At impact velocities $V \approx 80.0$ m/s, the spheres rebounded, causing only elastoplastic deformation on the plates, with no visual indication of fracture. Four M1 and three M2 plates were tested and exhibited a similar behaviour at this range of impact velocity, Fig. 5. Two deformation modes, global and local, were observed. Global deformation was almost axisymmetric, beginning with a rotation at the clamped region and a progressive bending until the impact point area. At this point, it was formed a local shinning spherical hollow with diameter smaller than the sphere. Global deformation of plates M1 contributed more to the maximum permanent displacement than for plates M2. Shear effects were more pronounced in the M2 plates.

A mechanical gauge of 0.01 mm resolution was used to measure the out-plane difference between the support and the impact point coordinates to evaluate the permanent deformation. A mean displacement, d, of the values measured in both sides of the plates was adopted. Fig. 6 depicts the results normalized by the respective plate thickness, H, as a function of the impact velocity normalized by respectively ballistic limit, $V_{\text{ballistic}}$. They indicated a linear relation between the maximum permanent displacement and impact velocity for both plates. Image shots indicated that, after the impact, a global elastic vibration of the plate occurs.

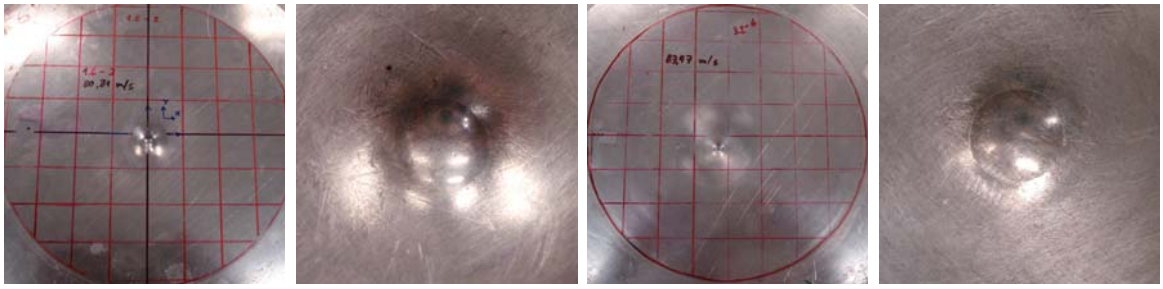

(a) M1 front view (b) M1 detail (c) M2 front view (d) M2 detail

Fig. 5 Front views and impact region details of M1 and M2 plates impacted at 81 m/s and 83 m/s, respectively

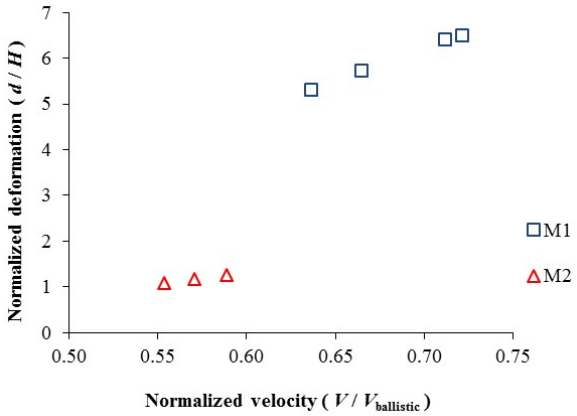

Fig. 6 Dimensionless maximum permanent deformation versus dimensionless impact velocity for plates M1 and M2

3.2 Ballistic limit determination

As the impact velocity increased, a macroscopic fracture appeared in the impact region. This can be observed in Figs. 7(a)-(b) and 8(a)-(b) for plates M1 and M2, respectively. The tests indicated that there is an impact threshold velocity that delimits the failure appearance. Note that, even in the presence of a macroscopic crack or petal formation, it is possible that the projectile does not go through the plate. In this case, the sphere simply rebounds, characterizing a partial perforation case.

For the M1 plates, the initial crack grew as the impact velocity increased, leading to the formation of one big petal and radial cracks, as observed in the total perforation case of the Figs. 7(c)-(d). It should be noted that the hole left by the sphere was smaller than its diameter due to the petal elastic return. Fig. 9 illustrates the total perforation process of the M1 plate.

In contrast, for the M2 plates, an increase in the impact velocity led to a second macroscopic crack formation, with a circular pattern around the impact region, visible only at the rear side of the plate Fig. 8(b). Further increase in the impact velocity caused the circular crack to grow until the formation of a plug with approximately half sphere-diameter size, Figs. 8(c)-(d). In this

(a) Front view (b) Rear view (c) Front view (d) Rear view

Fig. 7 Failure region detail of M1 plate: failure without perforation at 116 m/s (a-b); failure with total perforation at 129 m/s (c-d)

(a) Front view (b) Rear view (c) Front view (d) Rear view

Fig. 8 Failure region detail of M2 plate: failure without perforation at 110 m/s (a-b); failure with total perforation at 140 m/s (c-d)

configuration, the projectile can still rebound. Total perforation of the plate occurs only when radial cracks and elastic deformation make the hole instantaneously large enough to allow the sphere to pass through it. The verification of total perforation was done using the high speed camera images, as illustrated in Fig. 10 for the M2 plate. The final hole size was around 15\% smaller than the sphere diameter, indicating elastic recovery as in Gupta *et al.* (2006). It was noted that the M1 plate had a more pronounced membrane stretching behaviour than the M2 plates.

The velocity associated with the beginning of local failure and the ballistic limit were found from eighteen tests for the M1 plate and from seventeen tests for the M2, determining the limits of three zones: no failure, partial and total perforation, Fig. 11. From the test results it was possible to conclude that the ballistic limit was 120 m/s and 133 m/s for the M1 and M2 plates, respectively.

It should be noted that in one of the M1 plates there was a plug detachment. This result points out to the influence of other parameters on the deformation process. The plug detachment is in contrast with the results obtained by Gupta *et al.* (2006) for cylindrical projectiles with hemispherical end and 1.0 mm thick plates. It was observed plug formation, but the plug remained attached to the end of the petals. Only for flat end projectiles shear plugs were obtained. On the other hand, Borvik *et al.* (2002a) found the formation of plugs for 12 mm thick steel plates for both hemispherical and flat end projectiles. The plug shape obtained by Borvik *et al.* (1999), a truncated cone, whose larger basis is in the posterior side of the plate, was not observed here. In fact, the plug shape for plate M2 has its rear diameter smaller than the front one, where the sphere hits the plate.

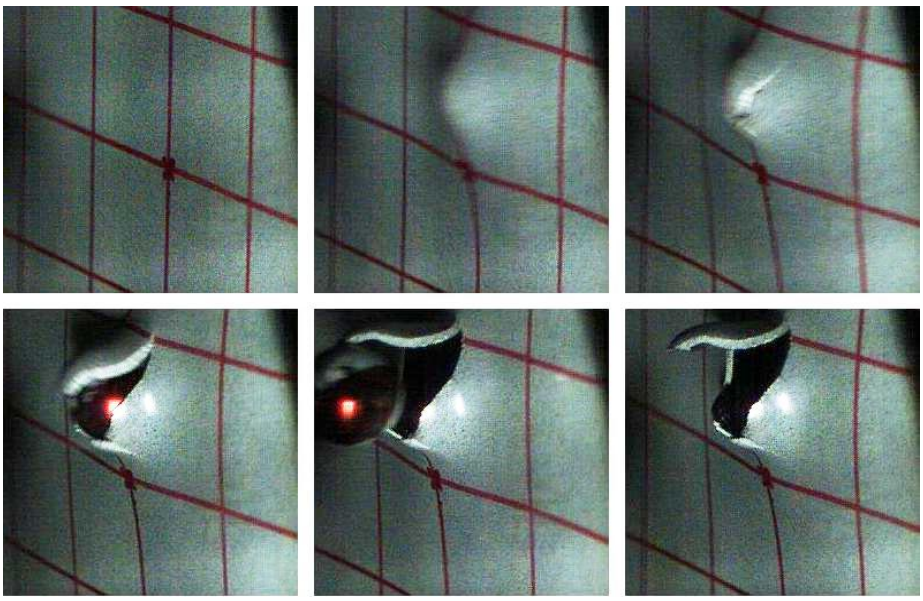

Fig. 9 Rear view of the perforation process of M1 plate by a 20 mm diameter rigid sphere travelling at 128 m/s

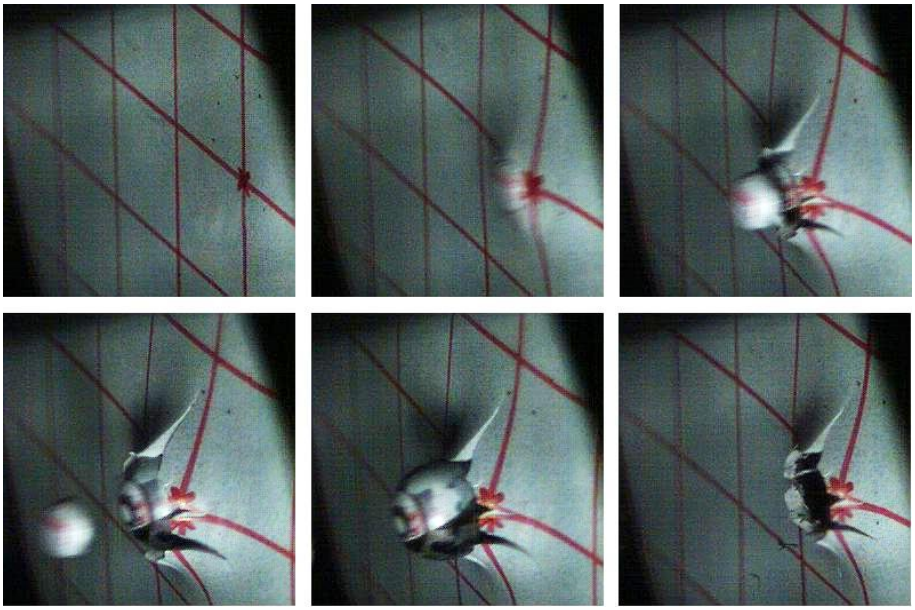

Fig. 10 Rear view of the perforation process of M2 plate by a 20 mm diameter rigid sphere travelling at 134 m/s. At 400 microseconds the plug detachment can be observed

4. Finite element model

The finite element method, as implemented in the software LS-DYNA version 970, was used to analyse numerically the plate impact tests. The aim is to investigate how the material models,

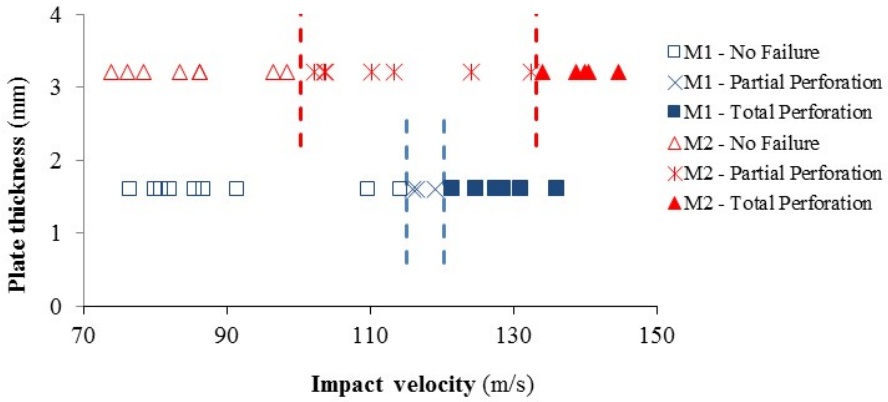

Fig. 11 Impact velocity ranges for three types of structural responses of plates M1 and M2

mesh characteristics and simulation parameters influence the numerical plate response for low and ballistic velocities. It is known that different element types and formulations can model different structural behaviours. Likewise, mesh discretization is important on the representation of the structure and wrong element sizes can lead to non feasible results. Additional factors as contact model, hourglass control, friction must also be investigated to evaluate the effect on the numerical predictions of structures under impact.

Three types of elements were used to generate the plate meshes in the program HYPERMESH: non-symmetric quadrilateral shell (2D) finite elements, non-symmetric hexahedral solid (3D) finite elements and axisymmetric (2D) finite elements. In the shell and solid cases, the hard spherical projectile was modelled as an analytical surface and the target mesh was formed by a central refined region, where the impact event takes place, and a less refined outer region. The transition between the regions was made gradual, as shown in Fig. 12(a), which presents a template mesh applied to the shell element case. 3D solid meshes were built by extrusion of this template. For the axisymmetric analysis, the sphere projectile was modelled using rigid elements, Fig. 12(b). A more refined mesh was also implemented in the impact region. All degrees of freedom of the nodes at the plate boundary were fixed to represent the clamped condition of the plate.

A study of mesh convergence was performed on the shell and solid meshes. Using the simplest material model and applying values from the literature for material data and default values for the simulation parameters, the ballistic velocity prediction was searched to evaluate the convergence. Fig. 13 presents these predictions normalized by the most refined mesh result. The results of these initial studies indicated that the ballistic limit is mesh dependent and led to the selection of the meshes to perform the numerical simulations of the impact tests. The element edge size of 0.26 mm (15 elements/mm^2) was chosen for the shell mesh. Due the computational limitations, the element edge size for the solid mesh was 0.52 mm (7 elements/mm^3), without convergence losses. For the axisymmetric mesh, an element size of 0.2 mm was used. Table 2 lists the main data regarding the various meshes.

Different element formulation were tested, similar to the convergence studies. The behaviour of the meshes at the impact region was qualitatively analysed during the perforation processes by comparisons with the experimental tests. Additionally, the computational time was taken in

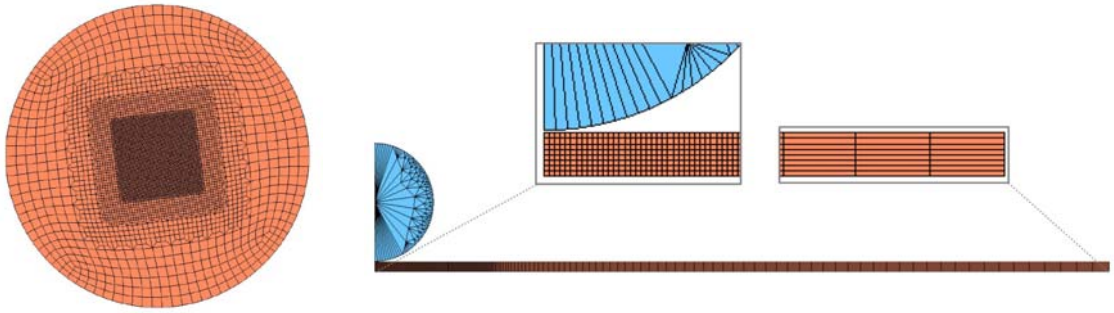

(a) Shell mesh (front view) (b) Axisymmetric and sphere meshes (cross section view)

Fig. 12 Different meshes used in simulations

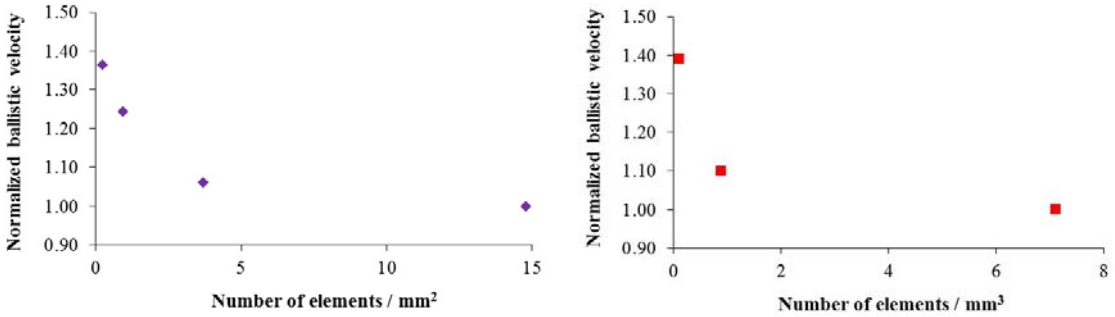

(a) Shell element mesh (b) Solid element mesh

Fig. 13 Evaluation of mesh convergence

account. From the obtained results, the Belytschko-Leviathan shell element with five integration points along the thickness was chosen to represent the plate. As for the 3D elements, the eight nodes hexahedral element was chosen with one integration point. No significant differences were found for the axisymmetric results. Following the suggestion by Hallquist (2006), the Galerkin axisymmetric element was selected.

For the non-axisymmetric meshes, the sphere was modelled as a rigid surface via a mathematical equation to define the contact master surface, as done by other authors (Teng and Wierzbicki 2006). For the axisymmetric case, the master surface was the boundary of the rigid element mesh of the sphere. Two contact parameters, the friction coefficient and the integration order were modified in various runs. Ravid and Bodner (1983) suggest a friction coefficient of 0.05 for metal interaction at high velocity and temperature, the same value used by Borvik *et al.* (2002b). Forrestal *et al.* (1988) noticed a layer of melted aluminium in the hole left by a projectile, so suggesting a close to zero friction coefficient between the projectile and the sheet. Given that the plates are thin and that the projectile is a sphere, it was decided to adopt a value of 0.02 for the friction coefficient. In some simulations, a value of 0.1 was used and no significant differences were found for the ballistic velocity, indicating a no friction dependency in these cases. Six possible values (0-5) were tested for the integration order in the contact model (LSTC 2003). This parameter affected just the results for the shell model and, judging qualitatively by the generated

Table 2 Mesh data

Mesh	Plate	Element edge size (mm)	Total number of elements	Number of elements per area or volume unit	Total number of nodes
Shell	M1 and M2	0.26	41,662	15 (per mm^2)	41,712
Solid	M1	0.52	62,136	7 (per mm^3)	77,916
	M2		124,272		140,248
Axisymmetric	M1	0.2	1,360	25 (per mm^2)	1,539
	M2		2,720		2,907

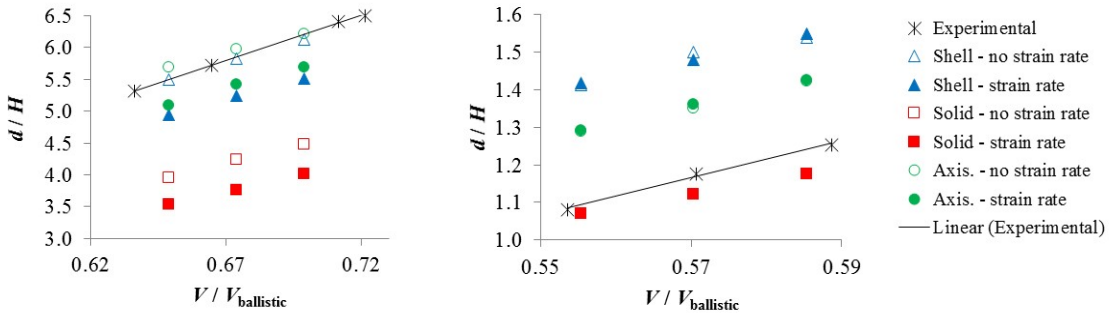

(a) M1 predictions (b) M2 predictions

Fig. 14 Maximum dimensionless permanent displacement versus the normalized impact velocity

symmetric failure pattern, it was chosen integration order 3.

The hourglass control for the selected shell element is automatic. For the solid elements, different hourglass controls were used. The standard LS-DYNA, the Flanagan-Belytschko and the Flanagan-Belytschko exact volumetric integrations yielded finite elements with too large distortions, while the Belytschko-Bindeman co-rotational formulation presented too large displacements. Good results were obtained by the Flanagan-Belytschko stiffness formulation and by the exact volumetric integration. The latter was chosen due the lower computational time. As for the axisymmetric elements, the results were practically the same regardless of formulation available on the LS-DYNA code.

The material properties were represented through the Lemaitre strain hardening and damage models and the Cowper-Symonds strain rate hardening model, both presented on the LS-DYNA code. The model material parameters were obtained from experimental tests and are listed in Table 1. The perforation process was modelled by element erosion LS-DYNA option and a damping parameter was added to the element formulation to represent the post-impact damped vibration of the plate.

5. Low velocity simulation results

Impact velocities of 78.0, 81.0 and 84.0 m/s for M1 plate and 74.0, 76.0 and 78.0 m/s for M2 plate were used to obtain the results for the low velocity experiments, when material failure did

Table 3 Percentage of elements among maximum plastic strain rate ranges, considering only the most refined mesh part. Results for the low velocity simulations

Plate	Mesh	Total number of elements	Up to 250 s^{-1}	250 s^{-1} to 1000 s^{-1}	1000 s^{-1} to 2500 s^{-1}	over 2500 s^{-1}
M1	Shell	12000	90 %	8 %	1 %	1 %
	Solid	45000	98 %	2 %	0 %	0 %
	Axi.	1000	61 %	21 %	18 %	0 %
M2	Shell	12000	98 %	2 %	0 %	0 %
	Solid	90000	99 %	1 %	0 %	0 %
	Axis.	2000	73 %	16 %	11 %	0 %

not occur and the sphere always rebounded after impact. The impact point was always on the mesh centre. Two set of simulations were performed, with and without the consideration of strain rate effects in the material model.

Fig. 14 presents the maximum out plane permanent displacements for plates M1 and M2 against the impact velocity, both variables made dimensionless with the plate thickness and the experimental ballistic velocity, respectively. The numerical results indicated a linear relation between these variables, in agreement with the experimental results shown in Fig. 6.

The shell mesh predicted best the final maximum deformation of the M1 plate, followed by the axisymmetric model, Fig. 14(a). In this case, the solid element mesh was too stiff when compared with the experimental results. However, for the M2 plate, the best prediction occurred for the 3D solid element, with the shell mesh yielding in the most flexible mesh, Fig. 14 (b).

Almost the same trend was found for the three meshes of M1 plate when dynamic effects were added to the material model, the meshes became stiffer. The M2 plate simulations, in contrast, exhibited results that are independent of the consideration of strain rate effects, except for a small variation for the shell mesh.

The strain rates that the elements were submitted on the simulations can be verified by the results presented in Table 3. Considering just the most refined part of the mesh and the maximum plastic strain rate to which each element was submitted during the simulation, Table 3 presents the distribution of the elements among plastic strain rate ranges. It can be observed, for shell and solid elements and for both M1 and M2 plates, almost all the elements were submitted to plastic strain rates below 250 s^{-1}. Just in the axisymmetric mesh simulation, significant part of the elements were submitted to strain rates up to 2500 s^{-1}.

The final maximum deformation of the plates was achieved simulating more 40 ms after the impact to allow plate vibration to disappear. It was 16 times longer than the ballistic simulations. The low processing cost of the axisymmetric element was evident, being 22 times less than the solid case.

6. Ballistic simulation results

Element erosion was used together with Lemaitre's damage model (Alves and Jones 2002) to evaluate numerical ballistic prediction of the plates M1 and M2. In this model, damage evolves with the accumulated plastic strain and the stress state. The element is removed from the analysis

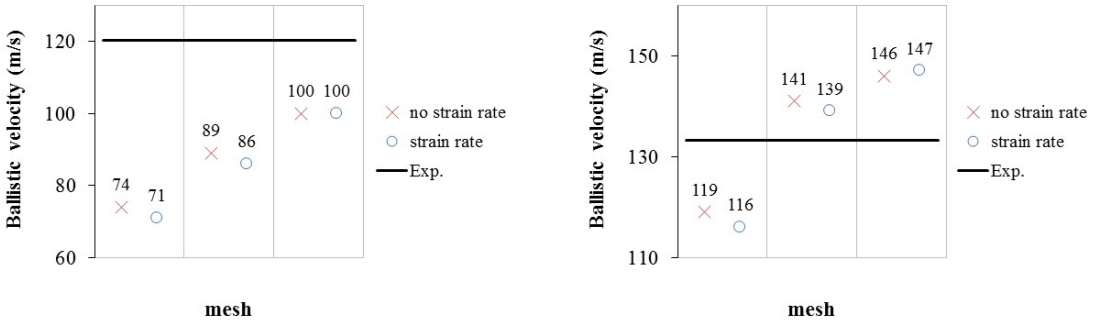

(a) M1 predictions (b) M2 predictions

Fig. 15 Numerical and experimental ballistic limits with and without strain rate effects

Table 4 Percentage of elements among maximum plastic strain rate ranges, considering only the most refined mesh part. Results for the perforation simulations

Plate	Mesh	Total number of elements	Up to 250 s^{-1}	250 s^{-1} to 1000 s^{-1}	1000 s^{-1} to 2500 s^{-1}	over 2500 s^{-1}
M1	Shell	12000	79 %	18 %	3 %	0 %
	Solid	45000	82 %	12 %	6 %	0 %
	Axi.	1000	50 %	20 %	28 %	2 %
M2	Shell	12000	60 %	34 %	6 %	0 %
	Solid	90000	73 %	21 %	6 %	0 %
	Axis.	2000	46 %	26 %	27 %	1 %

once its damage value reaches the critical one, determined from the material tests and presented in the Table 1. When indicated, the influence of the strain rate on the material response was taken into account via the Cowper-Symonds equation as in the non perforation simulations. The obtained results are presented in Fig. 15 and indicate that each element type lead to a different prediction. The impact velocity was varied in intervals of 2.5 m/s.

For the M1 plate, the prediction results are presented in Fig. 15(a) for the three finite element types and for the quasi-static and dynamic material models. The simulations for plates M1 predicted ballistic velocities 18 % to 41 % lower than the experimental value. The axisymmetric mesh was the model closest to the experimental results.

Fig. 15(b) presents the results for M2 plate. It can be observed that the shell elements yielded lower ballistic limits when compared with the experiments, by differences around 12 %. The other meshes led to predictions above the experimental results, around 6 % for solid elements and 11 % for the axisymmetric elements. Hence, the predictions for plate M2 were closer to the experimental values than for plate M1. The best predictions were within an error of 5 %, obtained when using solid elements with the inclusion of strain rate effects.

Considering the strain rate influence on the mesh response, for the axisymmetric mesh and both M1 and M2 plates, there was no significant differences in the predictions. However, considering the other two mesh types, the ballistic predictions were lower when material dynamic effects were considered. The M2 plates proved to be less sensitive to the consideration of dynamic effects on

the material response than M1. For plate M2, the differences between predictions were less than 2.6 %, while for M1 the difference were up to 4.1 %.

Table 4 presents the distribution of the elements among plastic strain rate ranges for the ballistic simulations. It can be observed that, for both M1 and M2 plates, almost all the elements were submitted to plastic strain rates below 2500 s^{-1}, regardless of the mesh type. Just in the axisymmetric mesh simulation, significant part of the elements were submitted to strain rates up to 2500 s^{-1}.

The simulations were run to represent 2.5 ms of the impact event, allowing total penetration of the sphere. The axisymmetric model yields a much short processing time, with the shell and solid meshes taking 3 and 85 times longer, respectively.

7. Discussion

The numerical simulations for ballistic and maximum permanent displacement of aluminium alloy clamped circular plates, subjected to the central impact of a hard sphere, yielded good results. The influence of various numerical parameters on these results, including finite element formulation and dynamic material model, was thoroughly investigated.

A mesh dependency was detected in the impact simulations, in line with the conclusions presented by Knight *et al.* (2000), Teng and Wierzbicki (2006). Despite this element size influence, there was a trend for the results to converge, as observed by Borvik *et al.* (2002b) for axisymmetric elements.

The transverse displacements of the plates was investigated without a damage model. The results were presented in Fig. 14. Note that the relative stiffness among the element types changed for the different materials. For M1 plate, the less stiff mesh was that of axisymmetric elements. For M2 plate, shell mesh became the most flexible. This can be attributed more to the difference in the thickness of the plates than the material properties. For shell meshes, there is no increase in the number of elements along the plate thickness when this variable increases. Whereas, for solid and axisymmetric meshes, the number of elements (and degrees of freedom) varies to represent plates with different thickness. This can be observed by the total number of elements in the most refined part of the meshes presented in Tables 3-4. Thereby, the difference on mesh representation of plate thickness can explain the changes on relative stiffness among shell, solid and axisymmetric meshes, when comparing plates M1 and M2.

In a next step in the analysis, damage was added to the model to perform the ballistic simulations, summarised in Fig. 15. The axisymmetric model presented the largest resistance to the sphere penetration, following by the solid and the shell meshes, in this order, for both M1 and M2 plates and independently of the consideration of the material dynamic behaviour.

The model with solid elements had a good agreement with the M2 plate, both for the prediction of the permanent displacement and for the ballistic limit, but did not for M1 plate. Being thicker than M1, M2 plate is subjected to more pronounced shear effects, which can be better captured by the solid element mesh.

The dynamic material characterization results, summarized on Table 1, indicated that the material of the M1 plate is more strain rate sensitive than of the M2 plate. For example, using Eq. (4), for ε_p=0.1, $\dot{\varepsilon}_p$ = 2500 s^{-1} and dynamic parameters of Table 1, the strain rate hardening increases the stress value by 15.5 % for the material of M1 plate and by 3.3 % for the M2 plate. This result contributed to the differences between the predictions when considering or not the

dynamic material models. Observing Figs. 14-15, it can be verified that major changes in the results, by including the strain rate effects, occur for M1 plates, even if the almost all elements were submitted to low strain rates, as observed in Table 3.

For the same plate type, comparing the results of Tables 3-4, it can be observed that in the ballistic simulation, more elements were submitted to strain rates above 250 s^{-1} and 1000 s^{-1} than in the deformation prediction case. For the M2 plate, the effect on the results followed the same trend, with the major changes occurring in the ballistic simulation. However, for the M1 plate, the major changes due the dynamic material model occurred on the permanent displacement predictions. The non-linear effect of the strain rate consideration on the damage model and element erosion process can be responsible for this difference on the results.

In general, strain rate hardening increased the stiffness for the low velocity simulations but decreased the ballistic velocity. It is important to note that the axisymmetric mesh was less sensitive to strain rate effects, even being its elements experiencing larger strain rates.

For both plates, three-dimensional analyses (solid and shell meshes) presented better qualitative results for the final plate configuration in the presence of failure than the two-dimensional one.

Considering both deformation and ballistic simulations, the best representation of the M1 plate behaviour was obtained when adopting the axisymmetric mesh. For the plate M2, the solid element mesh had the best performance. However, taking into account the computational cost, the advantage of the axisymmetric representation is indisputable. Probably because of this, axisymmetric meshes have been used to predict the ballistic limit (Borvik *et al.* 2002b, Roeder and Sun 2001, Teng and Wierzbicki 2006, Yadav *et al.* 2001) even with the limitation that it cannot represent well features like petal formation in the perforation region.

All these variations on the results point out to the complexity of the phenomenon under analysis. Indeed, the prediction of the ballistic velocity relies on a series of inter-dependent parameters, e.g. element type and size, constitutive material model, damage and penetration models etc., as here demonstrated.

8. Conclusions

The numerical simulations for ballistic and maximum permanent displacement of aluminium alloy clamped circular plates subjected to the central impact of a hard sphere yielded good results.

The perforation phenomenon of thin aluminium alloy plates by rigid spheres was studied both experimentally and numerically. The material properties were obtained under quasi-static and dynamic loads, which also included damage and failure parameters. Lemaitre and Cowper-Symonds material models were chosen to represent the entire behaviour of the materials under impact condition. The experimental ballistic limit of the plates was determined. At lower velocities its maximum permanent displacement was measured. The spheres penetrated the targets by a combination of petalling and plugging.

The sensitivity of several factors on the finite element results were studied. It is recommended that strain rate effects should be taking into consideration, even for materials exhibiting low strain rate sensitivity, as the alloys here tested. Also, it is important to pay close attention to the mesh, finite element type and other finite element parameters in order to obtain a good prediction for the penetration phenomenon. The Lemaitre model performed well and it is recommended for further studies on failure, bearing in mind that its parameters are relatively simple to be obtained. Failure under dynamic conditions was accordingly well predicted.

Acknowledgments

The financial support of the Brazilian research funding agencies FAPESP and CAPES is here acknowledged.

References

Alves, M. (2000), "Material constitutive law for large strains and strain rates", *J. Eng. Mech.*, **126**(2), 215-218.

Alves, M. and Jones, N. (2002), "Impact failure of beams using damage mechanics: Part I - theory", *Int. J. Impact Eng.*, **27**(8), 837-861.

Alves, M. and Karagiozova, D. (2007), "Correction of frictional effects on Hopkinson pressure bar compression tests", *Plasticity and Impact Mechanics*, Eds. Bruhns, O.T. and Meyers, E., Eur. Univ. Press, Bochum.

Alves, M., Karagiozova, D., Micheli, G.B. and Calle, M.A.G. (2012), "Limiting the influence of friction on the split Hopkinson pressure bar tests by using a ring specimen", *Int. J. Impact Eng.*, **49**, 130-141.

Ansys (1998), *Ansys Elements Reference*, release 5.5, Ansys Inc., Canonsburg, PA, USA.

Borvik, T., Langseth, M., Hopperstad, O.S. and Malo, K.A. (1999), "Ballistic penetration of steel plates", *Int. J. Impact Eng.*, **22**(9-10), 855-886.

Borvik, T., Hopperstad, O.S., Berstad, T. and Langseth, M. (2001a), "A computational model of viscoplasticity and ductile damage for impact and penetration", *Eur. J. Mech. A Solid*, **20**(5), 685-712.

Borvik, T., Hopperstad, O.S., Berstad, T. and Langseth, M. (2001b), "Numerical simulation of plugging failure in ballistic penetration", *Int. J. Solid. Struct.*, **38**(34-35), 6241-6264.

Borvik, T., Langseth, M., Hopperstad, O.S. and Malo, K.A. (2002a), "Perforation of 12 mm thick steel plates by 20 mm diameter projectiles with flat, hemispherical and conical noses. Part I: experimental study", *Int. J. Impact Eng.*, **27**(1), 19-35.

Borvik, T., Hopperstad, O.S., Berstad, T. and Langseth, M. (2002b), "Perforation of 12 mm thick steel plates by 20 mm diameter projectiles with flat, hemispherical and conical noses. Part II: numerical simulations", *Int. J. Impact Eng.*, **27**(1), 37-64.

Borvik, T., Clausen, A.H., Eriksson, M., Berstad, T., Hopperstad, O.S. and Langseth, M. (2005), "Experimental and numerical study on the perforation of AA6005-T6 panels", *Int. J. Impact Eng.*, **32**(1-4), 35-64.

Charoenphan, S. (2002), "Computer methods for modelling the progressive damage of composite material plates and tubes", Ph.D. Dissertation, Univ. Wisconsin-Madison, Madison.

Forrestal, M.J., Okajima, K. and Luk, V.K. (1998), "Penetration of 6061-T651 aluminum targets with rigid long rods", *J. Appl. Mech.*, **55**(4), 755-760.

Gupta, N.K., Iqbal, M.A. and Sekhon, G.S. (2006), "Experimental and numerical studies on the behavior of thin aluminum plates subjected to impact by blunt- and hemispherical-nosed projectiles", *Int. J. Impact Eng.*, **32**(12), 1921-1944.

Hallquist, J.O. (2006), *LS-DYNA Theory Manual*, Livermore Software Technology Corporation, Livermore, CA, USA.

Holmen, J.K., Johnsen, J., Jupp, S., Hopperstad, O.S. and Borvik, T. (2013), "Effects of heat treatment on the ballistic properties of AA6070 aluminium alloy", *Int. J. Impact Eng.*, **57**, 119-133.

Knight, N.F., Jaunky, N., Lawson, R.E. and Ambur, D.R. (2000), "Penetration simulation for uncontained engine debris impact on fuselage-like panels using LS-Dyna", *Finite Elem. Anal. Des.*, **36**(2), 99-133.

Kurtaran, H., Buyuk, M. and Eskandarian, A. (2003), "Ballistic impact simulation of GT model vehicle door using finite element method", *Theor. Appl. Fract. Mech.*, **40**(2), 113-121.

Lemaitre, J. (1992), *A Course on Damage Mechanics*, Springer-Verlag, Berlin, Germany.

Livermore Software Technology Corporation (2003), *LS-DYNA Keyword User's Manual*, (version 970),

LSTC, Livermore, CA, USA.
Ravid, M. and Bodner, S.R. (1993), "Dynamic perforation of viscoplastic plates by rigid projectiles", *Int. J. Eng. Sci.*, **21**(6), 577-591.
Recht, R.F. and Ipson, T.W. (1963), "Ballistic perforation dynamics", *J. Appl. Mech.*, **30**(3), 384-390.
Roeder, B.A. and Sun, C.T. (2001), "Dynamic penetration of alumina/aluminum laminates: experiments and modeling", *Int. J. Impact Eng.*, **25**(2), 169-185.
Sciuva, M.D., Frola, C. and Salvano, S. (2003), "Low and high velocity impact on Inconel 718 casting plates: ballistic limit and numerical correlation", *Int. J. Impact Eng.*, **28**(8), 849-876.
Song, B. and Chen, W. (2005), "Split Hopkinson pressure bar techniques for characterizing soft materials", *Lat. Am. J. Solid. Struct.*, **2**(2), 113-152.
Teng, X. and Wierzbicki, T. (2006), "Evaluation of six fracture models in high velocity perforation", *Eng. Fract. Mech.*, **73**(12), 1653-1678.
Tiwari, G., Iqbal M.A., Gupta P.K. and Gupta, N.K. (2014), "The ballistic resistance of thin aluminium plates with varying degrees of fixity along the circumference", *Int. J. Impact Eng.*, **74**, 46-56.
Yadav, S., Repetto, E.A., Ravichandran, G. and Ortiz, M. (2001), "A computational study of the influence of thermal softening on ballistic penetration in metals", *Int. J. Impact Eng.*, **25**(8), 787-803.

CC